UNIVERSITY OF CALIFORNIA,
IRVINE

Engineered microenvironments for biomolecule sensing in complex media

THESIS

submitted in partial satisfaction of the requirements
for the degree of

MASTER'S OF SCIENCE

in Physics

by

Alexandra Perebikovsky

Thesis Committee:
Professor Marc Madou, Chair
Professor Zuzanna Siwy
Professor Albert Siryaporn

2019

TABLE OF CONTENTS

LIST OF FIGURES

LIST OF TABLES

ACKNOWLEDGMENTS

First and foremost, I would like to thank the chair of my thesis committee, Marc Madou, for more than seven years of mentorship and friendship throughout my undergraduate and graduate career. I would also like to thank the other members of my thesis committee, Zuzanna Siwy and Albert Siryaporn, for their invaluable instruction and for the many thoughtful conversations we have had.

I would also like to thank my lab members, in particular Alexander Hwu, without whom this work would not be possible. His work ethic, organized experimental manner, and insight into the subject have made him one of my most trusted colleagues and an absolute pleasure to work with.

On a personal note, I would like to acknowledge my husband, Michiel Kosters and my parents, who have always pushed me to do more than I think I think I am capable of and who inspire me everyday to become a better person.

I would like to acknowledge the Laser Spectroscopy Lab for assistance with Raman Spectroscopy and Dr. Lisa Flanagan's Lab at the Sue and Bill Gross Stem Cell Center at UC Irvine for assisting with obtaining neural stem cells used in this project. I would also like to acknowledge Couryn Beleck and Keyence for help with obtaining high quality fluorescent images. SEM and XPS work was performed at the UC Irvine Materials Research Institute (IMRI) using instrumentation funded in part by the National Science Foundation Major ResearchInstrumentation Program [CHE-1338173]. I would also like to acknowledge the UC Irvine Institute for Design and Manufacturing Innovation for their funding and support.

I would like to acknowledge MDPI, Elsevier Ltd., the Electrochemical Society, and the American Chemical Society for granting permission to incorporate some of my previously published work into my dissertation.

ABSTRACT OF THE THESIS

Engineered microenvironments for biomolecule sensing in complex media

By

Alexandra Perebikovsky

Master's of Science in Physics

University of California, Irvine, 2019

Professor Marc Madou, Chair

For the last few decades, the field of carbon Microelectromechanical systems (CMEMS) has taken inspiration from the patterning and microfabrication techniques from microelectronics industry to create unique and intricate three dimensional carbon materials with a variety of properties and applications. Carbon has excellent electrochemical stability, chemical inertness, biocompatibility, and is able to be fabricated from a number of easily machinable polymer precursors. These features have allowed researchers to fabricate high performance electrochemical sensors, scaffolds for tissue engineering, batteries with excellent lithium intercalation capacity, and other microelectronic platforms.

In this work, microfabrication techniques are used to create a fragmented and graphitic carbon material that is used as a biosensor to detect iodide and Dopamine in complex fluids. The excellent microstructural properties of the material were able to detect both iodide and Dopamine at clinically relevant concentration levels in the presence of interfering ions in complex body fluids, making it an ideal biosensor.

Chapter 1

Introduction

Since the 1950s, the excellent electronic and mechanical properties of silicon have revolutionized the way we think of microelectronics and have paved the way for the development of microelectromechanical systems (MEMS) devices (1; 2). As this field has grown, new classes of materials have been developed that push the boundaries of miniaturization, have lower power consumption, better heat dissipation, are more environmentally friendly, and that are inert enough to interact with biological systems (3). One of the most attractive new classes of MEMS materials is carbon, particularly in applications such as electrochemical sensors (4), batteries (5), scaffolds for tissue engineering (6; 7; 8; 9), dielectrophoresis (10), fuel cells (11), and capacitors (12).

Carbon is one of the fundamental building blocks of life and is the fourth most abundant element in the universe. Its flexibility to form polymers and bond with many other elements at temperatures typically encountered on earth enables it to be present in all known living organisms. Due to its ability to hybridize and bond with itself, carbon comes in many versatile forms and allotropes, from diamond, one of the hardest bulk materials and an electrical insulator, to graphite, which has a soft structure and very high electrical conductivity (13).

The widely differing morphologies and crystalline structures of carbon have enabled development of materials and devices with vastly differing chemical, mechanical, and electrical uses. For example, hard carbons like graphite have long been used in lithium-ion battery applications due to their ability to intercalate Lithium, and amorphous, or glassy, carbons have been used frequently as electrochemical sensors due to their ability to form three dimensional shapes from polymer precursors and their wide electrochemical stability windows (14). Another critical aspect of carbon is its biocompatibility and chemical inertness, making it an ideal material for biological applications, such as biosensors, biomimetic scaffolds, and for the development of implantable devices.

1.1 Carbon from polymer precursors

The use of traditional manufacturing processes to shape carbon allotropes into microdevices is difficult due to the hard and brittle nature of most pyrolytic carbons. Similarly, technology derived from integrated circuits, such as the use of focused ion beam milling or reactive ion etching is expensive and time consuming, making it unpractical for the development of carbon microfeatures. However, rather than machining the final carbon itself, polymers containing carbon can be machined or patterned to create desirable microfeatures and miniature devices and then converted into carbon through a process known as pyrolysis.

During pyrolysis, an organic material or polymer is thermally decomposed in an oxygen-free environment into its carbon backbone. While most polymers change directly into a form of carbon that retains their original morphology without passing through a plastic phase, this process does lead to shrinkage of the polymer due to the decomposition of non-carbon molecules from its structure. This shrinkage is generally isotropic and consistent (repeatable), allowing for reproducible patterning and tight dimensional tolerances in the final product (15).

Typically, carbon derived from pyrolysis is known as "glassy" carbon due to its glass-like appearance when polished (16). While the exact structure of glassy carbon is still under debate, it is generally believed to have a fullerene-like structure, with discrete fragments of curved carbon sheets interspersed with pentagons and hexagons (17). This structure translates to its electromechanical properties. For example, glassy carbon exhibits good electrical and thermal conductivity, and has both low porosity and low permeability, making it chemically very inert and able to be etched at high temperatures under an oxygen atmosphere. These properties, combined with the carbon's wide electrochemical stability window and low background noise, makes it excellent for electrochemical applications, especially when the polymer precursor can be patterned into unique three-dimensional and high aspect ratio structures that improve its electrochemical kinetics (12; 14).

1.2 Photolithography

One of the most common methods for generating unique three-dimensional glassy carbon structures is through photolithography, or patterning of either a positive or negative polymeric photoresist. Multi-step lithographic processes can also be used to make complex structures and devices, shown in Figure 1.1. By controlling the photoresist composition, lithography conditions, the soft and hard bake times, and the pyrolysis ramping rates and temperature, a number of unique structures can be fabricated with different geometries, mechanical properties, and chemical properties (10; 18).

Figure 1.2 shows some of the unique structures that have been developed, including high aspect ratio carbon micropillars (19), suspended carbon wires (20), carbon fractals (21), and self-assembled carbon flowers (22). For example, a two-step photolithography process was used by Wang et. al. to produce high-aspect ratio carbon micropost arrays (20). The researchers further used the diffraction effect of UV light and different exposure rates to create

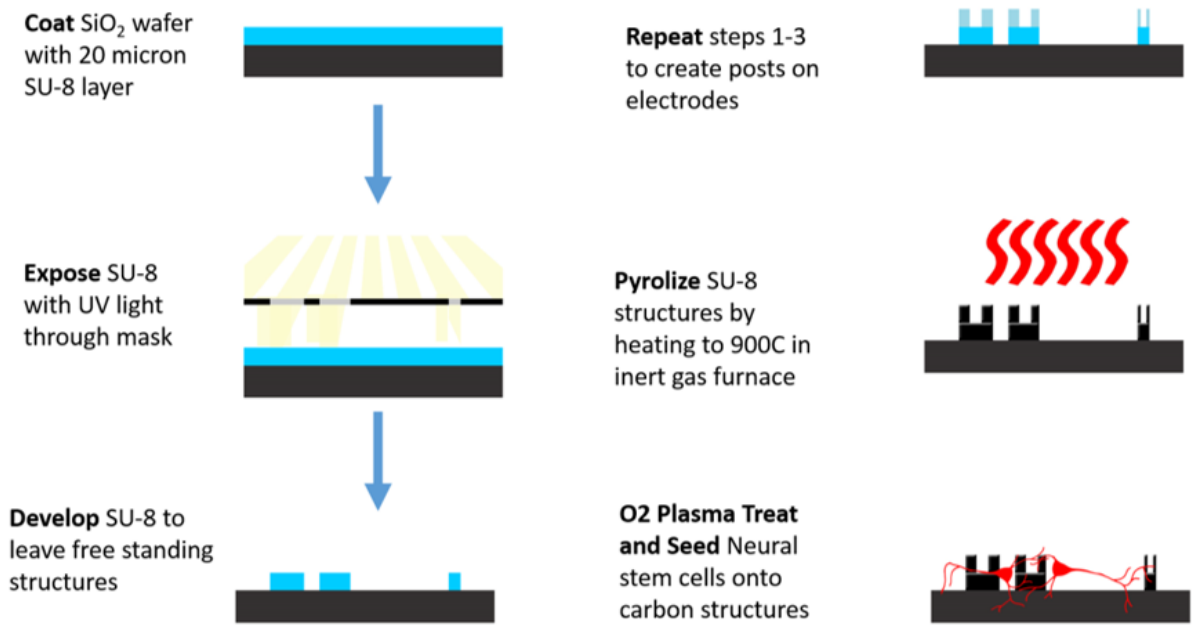

Figure 1.1: A two-step photolithography process for fabrication of carbon micropillars as a stem cell scaffold is shown.

suspended wires between the carbon posts. This unique structure yielded a high lithium ion charge discharge capacity and proved to have excellent electrochemical properties. Park et. al. created a carbon pillar with a high surface area, biomimetic, fractal-like structure by doping an epoxy-based negative photoresist, SU-8, with carbon nanofibers that include iron catalysts (21). This growth was retained following pyrolysis.

Photolithography was also used by Kamath et. al. to develop extremely senstive electrochemical sensors (23). Kamath fabricated a set of interdigitated electrode arrays (IDEAs) with finger spacing near 1 μm and a height of several microns. This three dimensional geometry enabled the use of redox cycling, depicted in Figure 1.3, where a redox active species is cycled between two working electrodes at opposing potentials multiple times before diffusing into the bulk. This enabled amplification factors 40 times greater compared with flat IDEA geometries. These examples show the remarkable capacity of cobmining photlithography with pyrolysis to create specialized carbon MEMS devices.

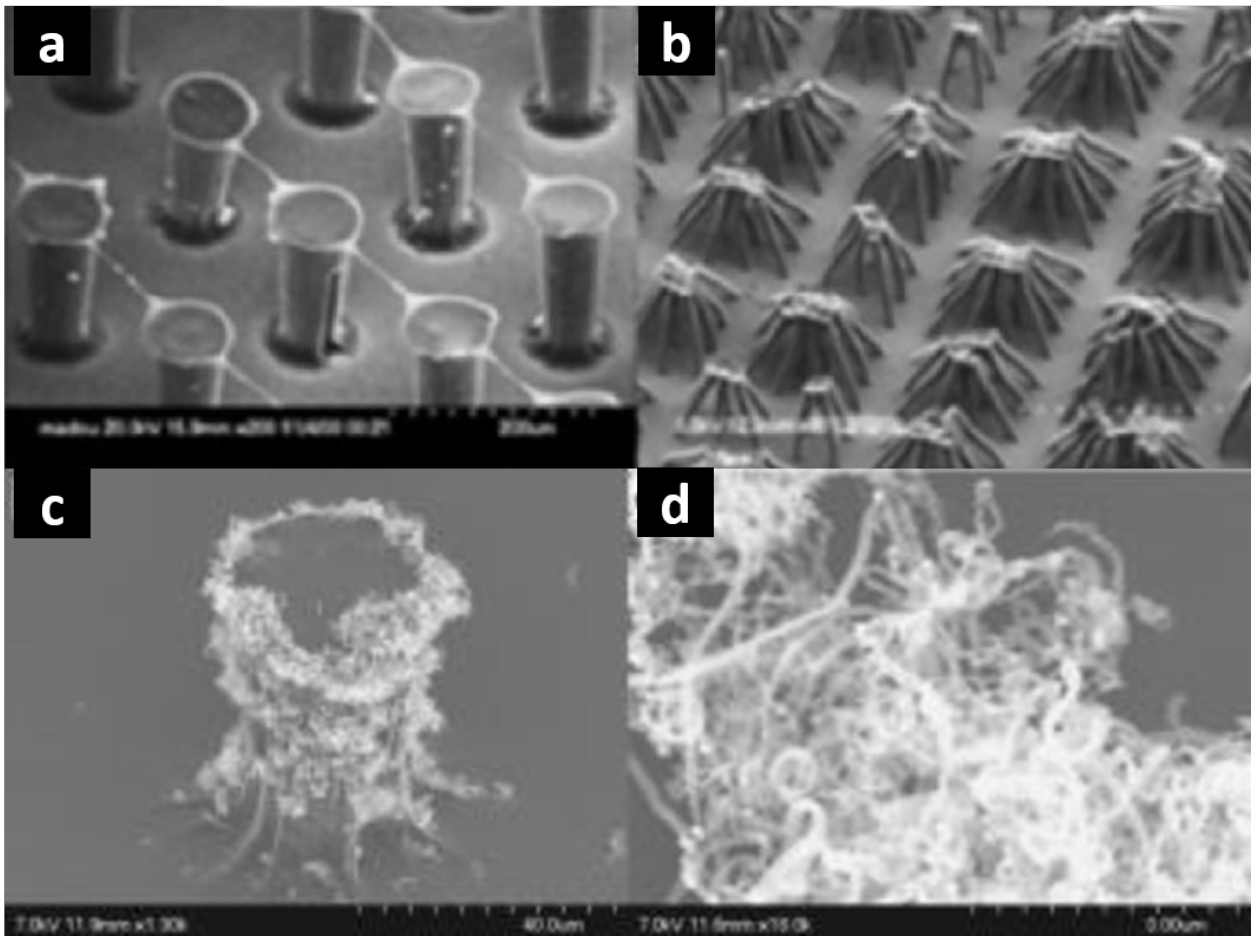

Figure 1.2: Unique MEMS structures created using photolithography: a.) carbon micropillars with suspended nanowires, b.) self-assembled carbon flowers, c.) fractal-like carbon micropillar made with doped photoresist, and d.) close up of fractal structure on micropillar.

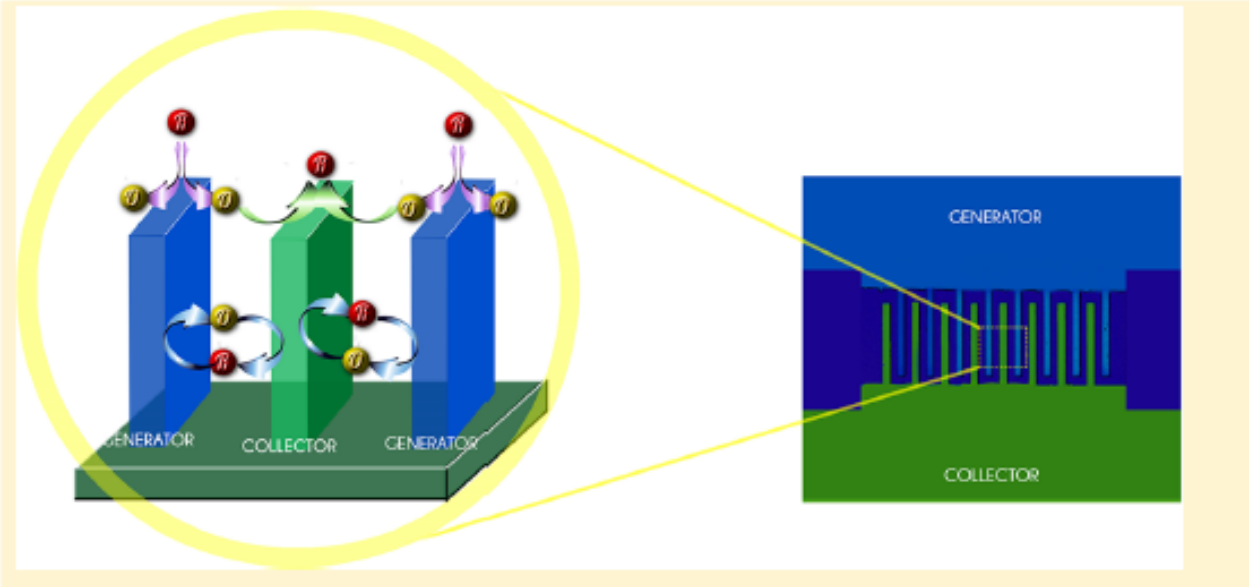

Figure 1.3: Schematic diagram depicting cycling of a redox active species between carbon IDEAs.

1.3 Electrospinning

Another carbon MEMS fabrication technique used extensively in this work is electrospinning, shown in Figure 1.4. Electrospinning relies on generating a large voltage gradient between a conductive polymer solution in a syringe and a conductive target (24). The large electrical field distorts a polymer droplet present at the tip of the syringe until it reaches a critical limit, where the electrostatic forces overcome surface tension forces within the droplet and pull a nanofiber jet out of the droplet.

Depending on the viscosity of the solution, distance from the target, temperature, and humidity, different fiber geometries can be created. For example, if the electrostatic forces are much larger than the viscous forces within the jet, a phenomenon called electrospraying occurs, where the polymer jet breaks apart into charged droplets that disperse onto the target. As the electrostatic force decreases, fibers of larger and larger diameters are formed. As the fibers travels toward the target and away from the polymer droplet, the charges in the fibers repel each other causing a whipping effect and creating a randomly oriented nanofiber

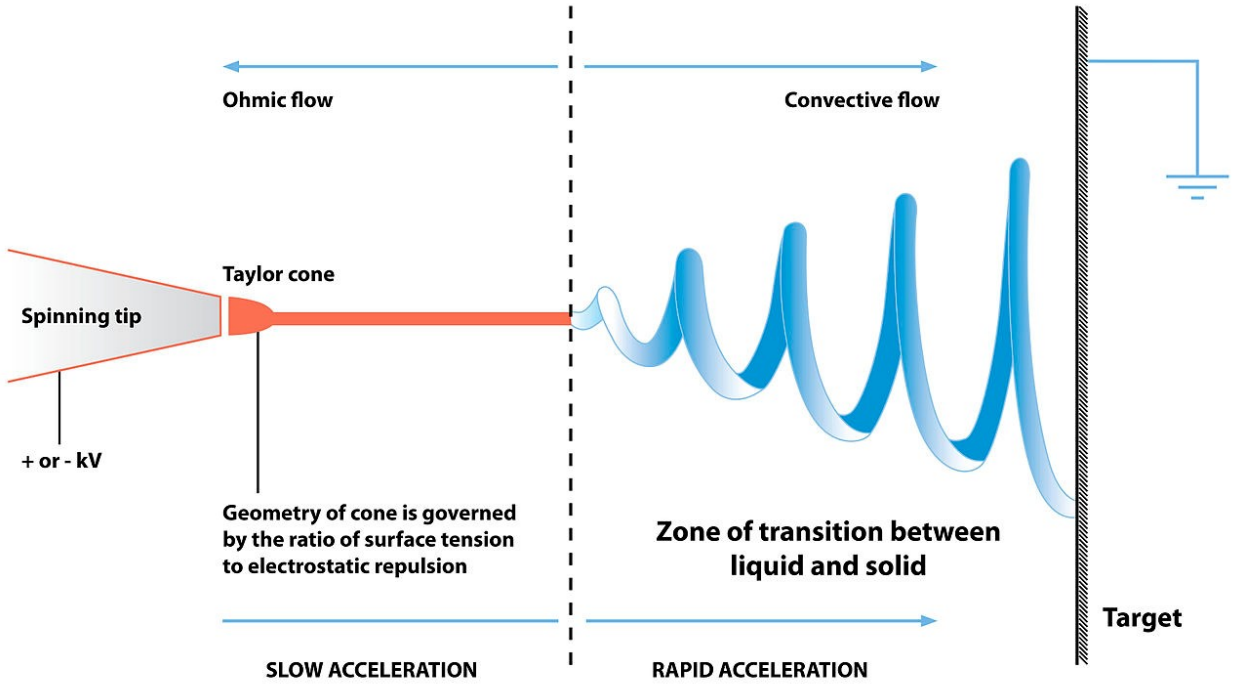

Figure 1.4: Schematic diagram depicting the electrospinning process.

matrix at the target. By using a rotating drum as a target, and rotating at a high enough RPM, aligned nanofibers can be created, shown in Figure **??**. By combining photolithography with different electrospinning parameters, structured nanofiber arrays, such as those shown in Figure 1.5 can be fabricated (25).

Electrospinning is also able to change the microstructure of the final pyrolized carbon as well, creating more graphitic carbon than that found in photolithography derived glassy carbon (26). The large shear forces during electrospinning pull on the coiled polymer chains in the jet, orienting them in the outermost diameter of the jet (27). This process can be enhanced using a rotating drum as the target to physically pull the nanowires, increasing the alignment of the polymer chains within the nanofibers. Finally, the addition of carbon nanotubes or similar structures to the polymer can create a template that helps uncoil the polymer chains and generates shear and drag forces during the electrospinning process (27; 28; 29). During pyrolysis, these uncoiled chains are retained, yielding a fragmented graphitic nanofiber

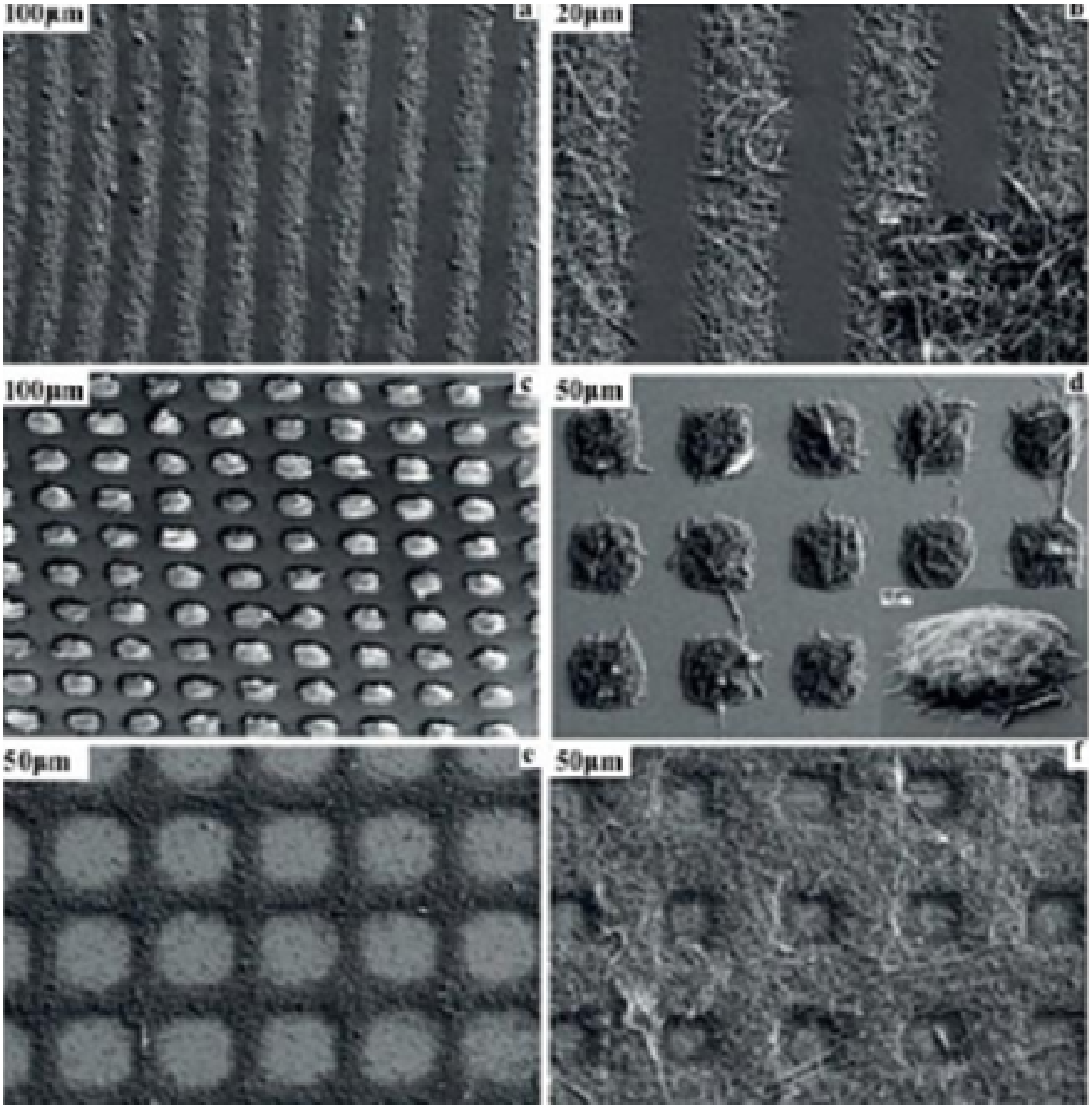

Figure 1.5: Control of electrospinning parameters to create patterned structures: a,b.) electrospun lines, c,d.) patterned nanofiber pillar arrays, and e,f.) connecting nanofiber squares and valleys.

structure. This fragmented graphitic structure comes with an abundance of electrochemically active edge planes, which translate directly into the electrical and chemical properties of the nanofiber mats.

In the following work, we describe the development of a unique carbon nanofiber material for the following applications: 1.) As a biosensor for the sensing of iodione in urine (see Chapter 2) and for the early detection of Dopamine in the presence of complex media (see Chapter 3).

Chapter 2

Rapid Iodine Sensing on Mechanically Treated Carbon Nanofibers

2.1 Background

Iodine is an essential micronutrient that plays a key role in thyroid hormone synthesis and brain development. Iodine deficiency disorder (IDD) is a major world health problem that leads to increased perinatal mortality, birth defects, hypothyroidism and a host of other functional and developmental abnormalities (30). For example, if iodine deficiency occurs during the most critical period of fetal brain development, the resulting thyroid failure leads to irreversible alterations in brain function (31).

One of the most critical aspects to controlling IDD is accurate and inexpensive monitoring of iodine concentration in physiological fluids. Since excess iodine is secreted in the urine of individuals, urinary iodine concentration is the main epidemiological indicator of IDD, with levels below 100 μg/L classified as deficient in healthy adults. During pregnancy, where IDD-induced neurological defects in the fetus are more common, optimal UI concentration

is defined between 150–250 μg/L (32).

While many methods have been developed to detect trace quantities of iodine, they are outdated, often expensive, and involve complex laboratory handling methods and instrumentation (33).

Commercially, urinary iodide concentration is exclusively measured colorimetrically by the Sandell-Kolthoff method, in which yellow cerium (IV) is reduced to cerium (III) in the presence of iodide ions. This method requires complicated sample preparation, involves a slow response time, and utilizes a toxic reagent that must be properly stored and disposed (34).

The goal in iodine monitoring research is to develop simple and sensitive methods for detection of iodine by using cost-effective probes that require no extra reagents or sample preparation. Ideally, these methods should have fast response times, low limits of detection, a wide dynamic range, and capability of detecting iodide ions in the presence of interfering substances. A number of studies on developing iodide sensors have been reported using various sensing nanomaterials (e.g., ZnO nanotubes-functionalized gold-coated glass, poly(3,4-ethylenedioxythiophene)/glassy carbon composite, plasticized polyvinyl chloride with two types of fluorescence, graphene quantum dots/silver nanocomposites) for ion selectivity and detection (35; 36; 37). However, the sensing material can be expensive (e.g., gold, silver), require additional treatments (e.g., chemical etching or reduction), or demand expensive optical instruments to measure signals.

A promising solution is to use electrochemical methods that take advantage of the electroactivity of iodide without adding any pretreatment steps. Silver working electrodes are commonly used for these electrochemical methods, exhibiting detection limits down to 40 nM and linear ranges from 0.2 to 1.6 μM [10]. However, silver electrodes need to be replaced frequently, since they operate by forming a silver iodide (AgI) precipitate on the surface.

This issue is also present in expensive platinum (Pt) or gold (Au) electrodes, where the detection of concentrations greater than or equal to 1 mM results in surface passivation of the electrode (38; 39).

An alternative approach is the development of iodide-sensitive electrodes using inexpensive carbon materials, such as glassy carbon and pyrolytic carbon fibers, which are chemically stable and exhibit a wide potential window. However, carbon electrodes often require post-synthesis processing (e.g., surface modification or inserting heteroatoms) to become effective iodine sensors. These methods can be complex, and, in the case of iodine, the resulting processes are transient. In one of the few related studies, Lowe et al. were able to detect low micromolar concentrations of iodide in a 0.1 mM sulfuric acid solution by exploiting the adsorption of iodide ions onto edge-plane pyrolytic graphite electrodes (40).

In this work, we demonstrate the detection of clinically relevant concentrations of iodide in synthetic urine and in the presence of interfering ions by using mechanically-treated pyrolytic carbon nanofiber (MCNF) electrodes. The unique microstructure of MCNF electrodes significantly improves its heterogeneous electron transfer rate (27), rendering them efficient, electrochemically active sensors. The MCNF material was used directly as an iodide selective electrode, without any post-processing or secondary activation methods. Cyclic voltammetry (CV) and differential pulse voltammetry (DPV) were used to characterize its efficacy as an iodine sensor. The enhanced electrochemical kinetics of MCNF electrodes in urine allow them to efficiently detect iodide ions and distinguish them from other interfering redox species that are present in synthetic urine. Based on the DPV characterization, MCNF electrodes exhibit 0.59 μM and 1.41 μM limits of iodine detection in 1X PBS and urine solutions, respectively. The results of this study demonstrate the promising capability of MCNF sensors for rapid, qualitative detection and monitoring of iodine in urine specimens.

2.2 Materials and Methods

2.2.1 Materials and Instruments

All chemicals used were of reagent grade. Multi-walled carbon nanotubes (MWCNT) and polyacrylonitrile (PAN, M.W. = 150,000 u) were purchased from Sigma Aldrich. N, N-dimethylformamide 99.9% (DMF), potassium iodide (KI), and phosphate buffered saline (PBS) tablets were obtained from Fisher Scientific. Artificial urine, pH 6.6, compliant with DIN EN 1616:1999, was purchased from Pickering Laboratories.

2.2.2 Electrode Fabrication

Polyacrylonitrile (PAN, M.W. = 150,000 g/mol, Sigma Aldrich) was mixed with N,N-dimethylformamide (DMF 99.9%, Fisher Chemical) and multi-walled carbon nanotubes (MWCNT) to produce 8% (v/v) PAN and 1% (w/v) MWCNT-DMF solution. This precursor solution was spun by a far-field electrospinning technique using 12 kV electrical potential and 0.9 mL/h flow rate. The PAN-CNT nanofiber mats were then mechanically rolled using a Dayton's DC Speed Control Roller. The resulting mat was stabilized at 280° C in air, and pyrolyzed at 1000° C under nitrogen flow, to produce the mechanically treated carbon nanofibers (MCNF).

As described comprehensively in our previous report, the addition of MWCNT to PAN DMF solution introduces dielectrophoretic forces in the electrospinning process, and results in velocity gradients at the interface of the MWCNTs and polymer chains. This phenomenon produces localized shear stress fields at the surface of MWCNTs, thus unwinding and aligning PAN molecular chains within these zones. Upon pyrolysis, our fabrication strategy results in a unique graphitic microstructure, which is rich in carbon edge planes and ni-

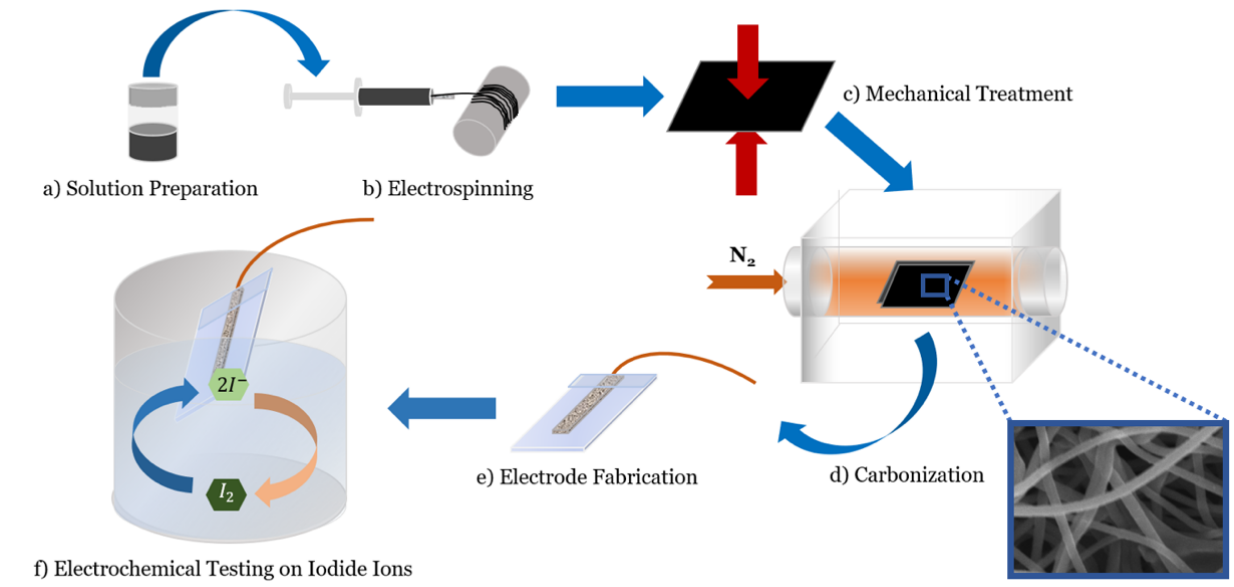

Figure 2.1: Schematic diagram of the fabrication and electrochemical testing of the MCNF electrodes. (a,b) PAN-CNT solution is electrospun onto a rotating drum via a far-field electrospinning technique. (c) the resulting nanofibers are treated with compressive, mechanical stress; (d) mechanically-treated carbon nanofibers (MCNF) are carbonized at 1000° C under nitrogen flow; (e,f) MCNF's are cut into electrodes and electrochemically tested in 1X PBS buffer and synthetic urine with different iodide concentrations.

trogen heteroatoms. It is important to note that the presence of edge planes is critical to electrochemical performance of carbon materials. While CNTs has a graphitic microstructure, it is mostly comprised of basal planes, and therefore are not electrochemically as active as "fragmented" graphitic structures, which contain a high quantity of electroactive sites. Accordingly, the role of MWCNT is to align PAN precursor molecular chains that, in combination with applied mechanical stresses during the stabilization, will generate fragmented graphitic microstructure with enhanced electrochemical response. The MCNF material was directly used to fabricate carbon electrodes with no additional post-synthesis processing. Figure 2.1 summarizes the fabrication of the MCNF electrodes.

2.2.3 Electrochemical Characterization

Electrochemical measurements were conducted using a Princeton Applied Research VersaSTAT 4 Potentiostat running VersaStudio 2.48.5 software. All electrochemical experiments were run in 1X PBS solution, which was made by dissolving prepackaged tablets in deionized water; one tablet in 200 mL of deionized water yields 0.01 M phosphate buffer, 0.0027 M potassium chloride, and 0.137 M sodium chloride at pH 7.4. An Ag/AgCl electrode in saturated 3 M NaCl solution was used as the reference electrode, and glassy carbon was used as the counter electrode for all electrochemical experiments. Cyclic voltammetry experiments were performed using 1 mM KI in 1X PBS and in synthetic urine. Electrochemical Impedance Spectroscopy (EIS) was performed after each cyclic voltammetry measurement to determine the active surface area of each electrode. Differential pulse voltammetry (DPV) experiments were run in both 1X PBS solution and synthetic urine with stepwise additions of KI, resulting in KI concentrations ranging from 100 nM to 1 mM.

2.3 Results and Discussion

2.3.1 Materials Characterization

A set of materials characterizations, including Raman and XPS spectroscopies, and electron microscopy, was conducted to determine the chemical and structural properties of MCNF.

In Figure 2.2b, the scanning electron micrographs of the resulting MCNF shows these nanofibers are relatively uniform and have an average diameter of 250 nm. The averaged Raman spectrum of the MCNF were obtained from 100 spectra of random areas on each carbon electrode to investigate the level of graphitization of the carbon materials. The D peak at 1350 cm^{-1}, and G peak at 1600 cm^{-1} correlate with structural disorder and crystalline

graphitic phase, respectively.

Accordingly, the I_d/I_g peak intensity ratio—a standard criterion for assessing the quality of carbon—is determined to be 0.86, showing the graphitic quality to be higher compared to typical untreated PAN-based carbon nanofibers. However, graphitization alone is not enough to enhance the electrochemical performance of carbon materials. Instead, the presence of the right graphitic "disorders" and heteroatoms play a major role in the fast-electrochemical kinetics of carbon materials. As shown in our previous reports transmission electron microscopy (TEM) shows that the main source of disorders in MCNF are from carbon edge plane, which provide electroactive sites for efficient electron transfer (27; 41). X-ray photoelectron spectroscopy (XPS) allows us to search for the presence of heteroatoms via analyzing various carbon bonds within the carbon structure (Figure 2.2c). The table in Figure 2.2d breaks down the elemental composition of MCNF, revealing a significant quantity of various nitrogen groups. These nitrogen groups consist of primarily pyridinic and graphitic, which have been associated with enhancing the electrocatalysis of graphitic carbons (42; 43).

2.3.2 Electrochemical Characterization

Cyclic Voltammetry

The cyclic voltammogram (CV) shows the electrochemical response of MCNF electrodes in the presence of 1 mM potassium iodide in 1X PBS and in synthetic urine, summarized in Figure 2.3. In both media, the presence of redox peaks (I/i) and (II/ii) is attributed to a two-step redox reaction, summarized in the equations below:

Peak I shows the oxidation of iodide ions (I^-) to triiodide (I_3^-) and peak II shows the oxidation of triiodide to iodine (I_2). The redox potential (E_0) for a redox couple allows us to assess the kinetic behavior of an electrochemical reaction. For the iodide/triiodide

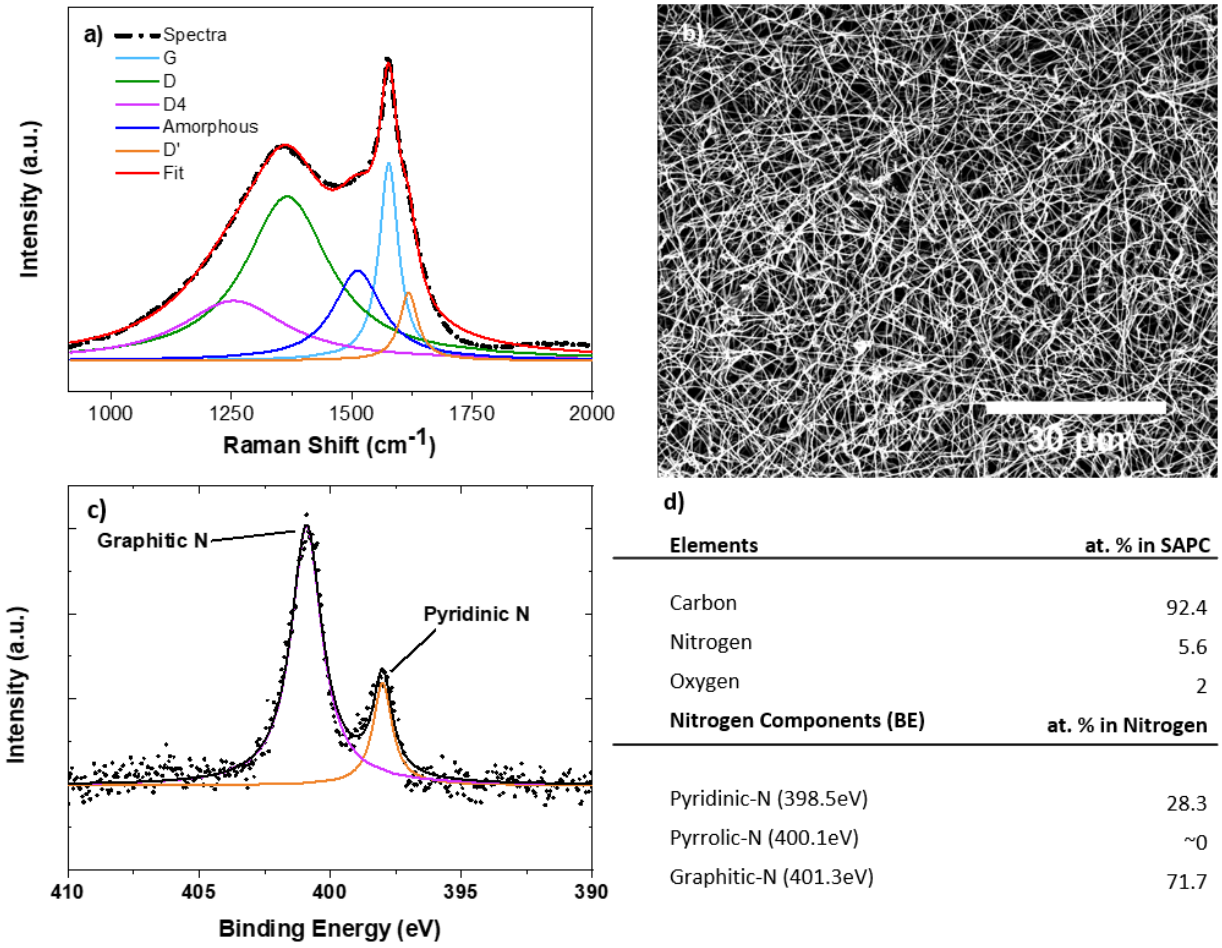

d)

Elements	at. % in SAPC
Carbon	92.4
Nitrogen	5.6
Oxygen	2
Nitrogen Components (BE)	**at. % in Nitrogen**
Pyridinic-N (398.5eV)	28.3
Pyrrolic-N (400.1eV)	~0
Graphitic-N (401.3eV)	71.7

Figure 2.2: (a) Raman spectrum with fitted Lorentzian curves for MCNF electrodes. More than 100 Raman spectra collections (λ excitation = 532 nm) were averaged to analyze MCNF; (b) Scanning electron micrograph of MCNF's; (c) XPS N 1s peak of MCNF; (d) Elemental composition of the carbon electrodes as analyzed from XPS.

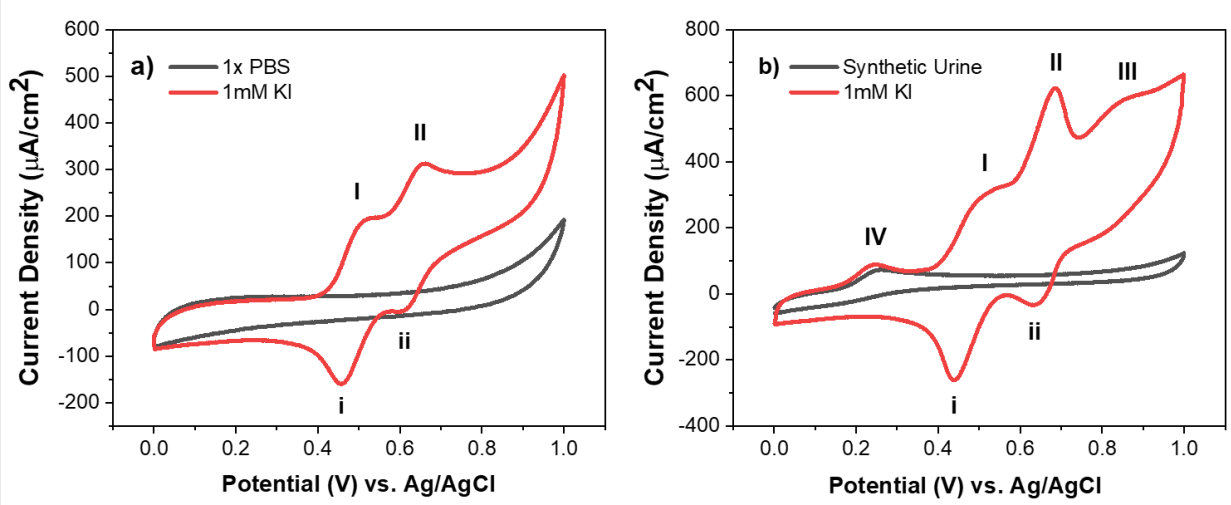

Figure 2.3: Cyclic voltammograms of 1 mM potassium iodide in (a) 1X PBS and (b) synthetic urine with a scan rate of 5 mV/s. The two-redox reactions of iodide ions are shown as (I)/(II) and (i)/(ii), respectively in both 1X PBS and synthetic urine. The additional peaks are observed in Figure 3b attributed to the oxidation of unknown species occurring in the presence of potassium iodide (III) or the oxidation of creatinine in synthetic urine (IV).

redox reaction (I/i) in 1X PBS and in synthetic urine, the calculated E_0 values were 0.486 +/- 0.004 V and 0.476 $\pm$ 0.002 V, respectively. This minor shift in the redox potentials shows that the redox reaction of (I/i) remains largely unaffected by a change in environment from 1X PBS to synthetic urine. This observation was corroborated by comparing the peak intensity of the reaction in both solvents, measured to be 165 +/- 2 $\mu A/cm^2$ in 1x PBS and 170 +/- 11 $\mu A/cm^2$, in synthetic urine. Similarly, very little shift in the E_0 values of the triiodide to iodine (peak II/ii) redox reaction was observed (0.636 +/- 0.003 V and 0.639 +/- 0.002 V in 1X PBS and synthetic urine, respectively). In this case, however, a 19% increase in current density was observed in synthetic urine (140 +/- 5 $\mu A/cm^2$ in synthetic urine vs. 114 +/- 2 $\mu A/cm^2$ in 1X PBS). In CV, the current density is directly related to the ionic flux, determined by the diffusion and transport of ions to the surface of the electrode. This increase in current density may be caused by the presence of heterogeneous chemical compounds that facilitated the transport of triiodide ions and promoted the overall oxidation of triiodide.

The additional peaks (III) and (IV) further confirm the presence of heterogeneous species in synthetic urine. In Figure 3b, peak (IV) was seen with and without the presence of 1 mM potassium iodide, indicating that the peak comes from endogenous chemical compounds that also participate in the overall redox system. Based on the work of Lopez-Giacoman et al., the observed peak indicates the oxidation of creatinine, an essential marker for diagnosing kidney-related disorders or muscular dystrophies (44). Conversely, peak (III) was only observed when 1 mM KI was added to synthetic urine. This electrochemical phenomenon suggests that additional urinary species are being electrochemically oxidized in the presence of iodide ions. Further investigation of the exact oxidation process occurring at peak III is needed. Overall, based on CV results, MCNF electrodes have demonstrated effective selectivity towards iodide ions within complex biological media.

Differential Pulse Voltammetry

Differential pulse voltammetry (DPV) is a highly sensitive pulse voltammetric technique that can discriminate against capacitive current in favor of oxidation or reduction currents, yielding sharp, well-defined peaks at lower concentrations of analyte. As a result, we were able to apply this technique to the quantitative analysis of iodide in both 1X PBS buffer and synthetic urine. DPV was run with a scan rate of 25 mV/s, a pulse height of 75 mV, and pulse width of 0.05 s. Analysis was performed by gradually increasing the concentration of KI in 1X PBS or synthetic urine and measuring the current density of corresponding peak (II) with respect to the background. The components of synthetic urine and their corresponding concentrations are listed in Table 2.1.

The calibration plots in Figure 2.4 show a linear relationship between the peak height and concentration of iodide ions. Statistical analysis of the data corroborated this linearity by yielding high values of the correlation coefficient in the concentration range from 5 μM to 700 μM ($R^2 > 0.99$ for both 1X PBS and synthetic urine). This linearity allows us to determine

Component	Concentration (g/L)
Urea	25
Sodium Chloride	9
Disodium Hydrogen Orthophosphate, anhydrous	2.5
Potassium Dihydrogen Orthophosphate	2.5
Ammonium Chloride	3
Creatinine	2
Sodium Sulphite, hydrated	3

Table 2.1: Chemical composition of synthetic urine.

the limit of detection (LOD) and dynamic range of our MCNF. The LOD quantifies the lowest amount of analyte that can be detected using MCNF electrodes. LOD values were calculated according to the following equation (45):

where σ is the standard deviation of the data and S is the sensitivity, found by calculating the slope of the calibration curve. Using this equation, an LOD of .591 μM was estimated for MCNF in 1X PBS and an LOD of 1.41 M in synthetic urine. For healthy adults, the WHO defines IDD as a urinary iodide concentration below 1.58 μM (<100 μg/L). The full spectrum of IDD is classified as mild deficiency, moderate deficiency <0.77 μM (<40 μg/L), and severe deficiency <0.32 μM (<20 μg/L). While an array of different sensors is required to fully determine the levels of IDD, our MCNF electrodes excel as rapid and inexpensive, qualitative sensors for IDD, particularly in complex urine samples.

The sensitivity of our MCNF electrode towards iodide ions in the presence of interfering ions was demonstrated by conducting DPV in synthetic urine. Table 2.1 shows the components of the synthetic urine used in the voltammetry experiments, with the principal interfering ions (i.e., urea and creatinine) present in concentrations similar to those of clinical urine specimens (46; 47). Figure 2.4b indicates that our MCNF electrode continues to demonstrate selectivity and sensitivity towards iodide ions in the presence of clinically appropriate concentrations of these interfering ions. The selectivity of our sensor for iodide ions is further supported by the CV obtained in synthetic urine. The results of the DPV and CV demonstrate that

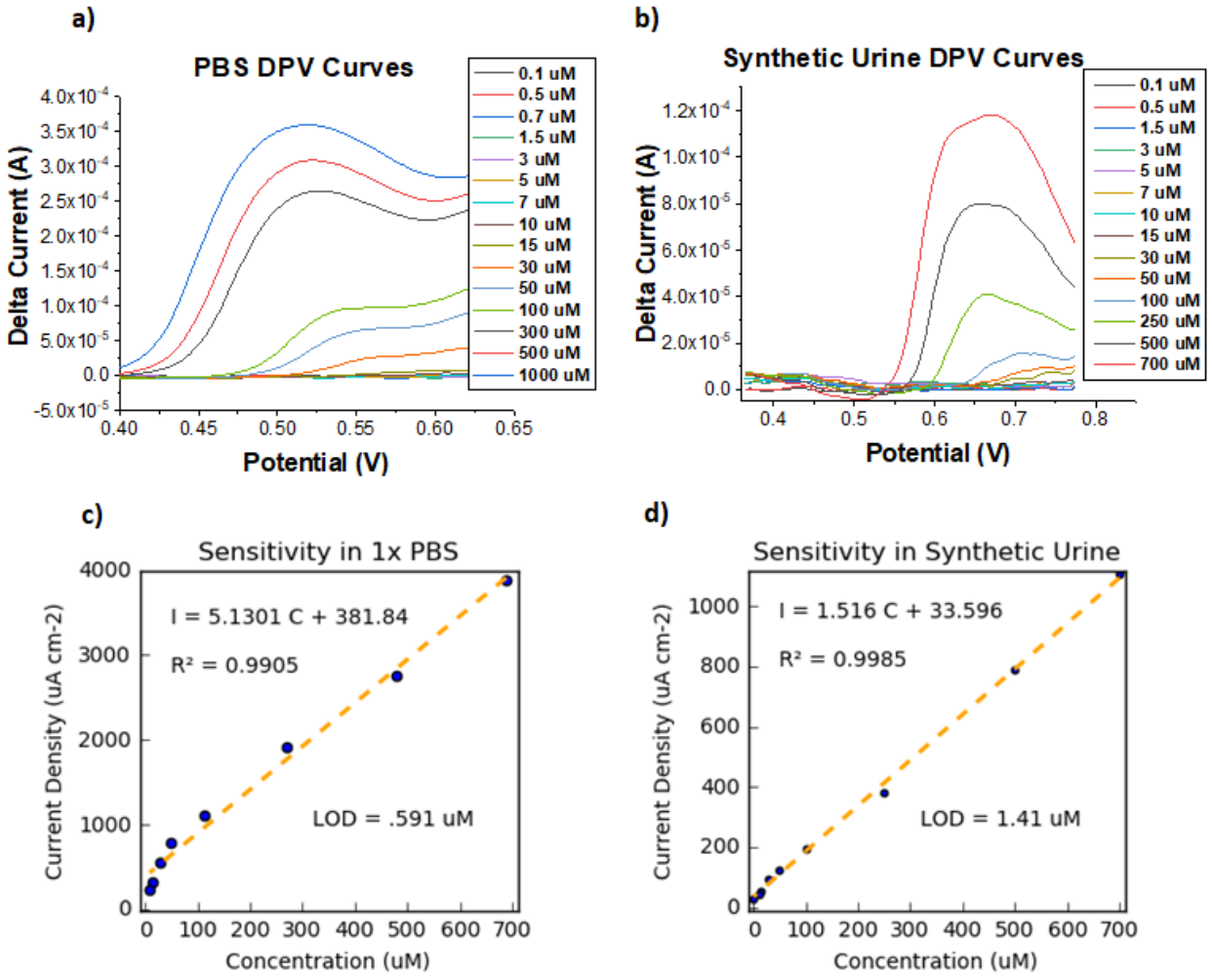

Figure 2.4: DPV curves (background subtracted) and calibration plots based on DPV data showing iodide sensitivity in 1X PBS (a,c) and synthetic urine (b,d). The regression equation, correlation coefficient, and estimated LOD are also shown on the plot.

our material not only remains sufficiently sensitive to iodide ions in complex media, but also differentiates among various interfering species in solution.

Moreover, the wide dynamic range of our sensor allows us to address additional iodine disorders occurring at excessive iodine concentrations. Excessive iodine, defined at concentrations greater than 4.73 μM (>300 μg/L), contributes to adverse health consequences such as hyperthyroidism and autoimmune thyroid disease (48). These results, combined with the advantage of minimal sample preparation needed for testing, demonstrate the promising nature of MCNF sensors as an ideal point-of-care (POC) platform, particularly in rural areas with limited access to complex biomedical laboratories.

2.4 Conclusion

We investigated the capability of mechanically-treated carbon nanofibers (MCNF) as a promising platform for diagnosing both iodine deficiency (IDD) and iodine excess in urine. IDD is the most important preventable cause of neurological deficiencies worldwide and excess iodine can lead to thyroid-related disorders (31),(36). The unique microstructure and composition of MCNF electrodes make them uniquely suited for electrochemical sensing of iodine. The cyclic voltammograms of MCNF electrodes in synthetic urine and PBS buffer demonstrate their efficacy in sensing and differentiating iodide ions from other interfering urinary species, without the need for complicated sample preparation and post-processing of the probe. Further quantitative analysis by DPV tests reveals that MCNF electrodes exhibit wide dynamic ranges that allow detection of excess iodine and limits of detection that allow for diagnosis of mild IDD. This work represents a proof of concept for using MCNF electrodes as POC sensors for iodine screening, particularly in low-resource setting areas.

Chapter 3

Mechanically treated Carbon nanofibers for early detection of Dopamine

3.1 Background

Dopamine (DA) is a neurotransmitter that modulates critical functions of the central nervous system and also plays an important role in metabolic, cardiovascular, and hormonal systems (49). Insufficient DA is responsible for many devastating diseases, such as Parkinson's, Alzheimer's, Huntington's and even depression. Therefore, developing platforms for selective and sensitive detection of DA, especially in complex biological samples, is critical.

Standard methods for DA detection include immunoassays such as Enzyme Linked Immunosorbant Assay (ELISA) and column methods such as High performance liquid chromotography (HPLC). However, these methods can be time consuming, expensive, and laborious, limiting their use for early detection of disorders involving Dopamine. Since DA is an elec-

troactive compound, electrochemical detection has recently become an attractive method for it's detection (50; 51; 19). Furthermore, DA is highly redox active, making its electrochemical detection possible without the need for extra redox couples or enzymes to mediate the reaction.

However, electrochemical detection of DA in complex body fluids, such as blood, can be tricky due to the presence of interfering compounds such as ascorbic acid (AA) and uric acid (UA) (42; 11). On the other hand, changes in the concentration levels of AA, UA, and DA have been directly linked to the presence of neurodegenerative diseases such as Parkinson's (52; 49). These compounds have overlapping oxidation potentials with most conventional electrode materials such as gold, platinum, or carbon, making their selective detection difficult. Furthermore, DA is present in low concentrations in most body fluids, necessitating highly sensitive electrodes for its successful detection. Therefore, the development of highly sensitive and selective electrodes for the detection of DA has long been a goal in this field of research.

Since electrochemistry is a largely interfacial phenomenon, various techniques, such as surface modification using synthesized nanoparticles, polishing, heat treatment, and laser irraidation, have been employed to improve kinetics of electrode materials (14; 53). The core of this strategy is to either increase the electroactive surface area of the electrode or to generate surface and structural defects that introduce new electronic states at energy levels around the E^0 of the redox systems of interest (12). Consequently, these defects function as favorable sites for electron transfer. Another technique includes the introduction of heteroatoms, such as nitrogen, which act as electron donors, improving electrochemical performance (54). This technique has been used favorably in carbon electrodes to generate carbon materials with n-type conductivity.

While these approaches do improve the sensitivity and kinetics of electrodes, they can be time consuming, involve expensive and laborious synthesis or processing steps, and can be

costly to fabricate (53; 55). Furthermore, many surface modifications are transient in nature, requiring electrodes to be used immediately following surface modification.

To address these challenges, we developed a porous, 3D carbon material with a graphitic microstructure that is both highly conductive and naturally rich in nitrogen heteroatoms, making it ideal for the electrochemical detection of DA. To create a carbon material with ideal three dimensional structure and properties, PAN polymer nanofibers, infused with carbon nanotubes, were deposited using controlled electrospinning. This material was then mechanically compressed and pyrolyzed at low termperatures to allow retention of the nitrogen heteroatoms naturally found in PAN polymer in the final carbon. The final carbon exhibited a uniquely graphitized structure, abundant in edge planes and nitrogen heteroatoms, which translates into its electrochemical kinetics. To optmize the material for the detection of DA, different concentrations of CNTs were mixed with PAN polymer. The optimal percentage of CNTs was determined by finding the sensitivity and limit of detection (LOD) of each resulting electrode for DA. Finally, the electrode with the highest electrocatalytic performance was used for selective detection of Dopamine in the presence of multiple adsorptive species, such as uric acid and ascorbic acid.

3.2 Experimental

3.2.1 Material Fabrication

Polyacrylonitrile (PAN; MW 150,000 u) (Millipore-Sigma, Catalog Number 181315) and multi-walled carbon nanotubes (MWCNTs) (Millipore-Sigma, Catalog Number 659258) were dissolved with anhydrous dimethylformamide (DMF; Fisher Scientific). Briefly, PAN was dissolved in DMF at 60 °C using a stirred-hot plate. Once a homogenous solution was obtained, MWCNTs was added and stirred overnight (12 hours) until evenly dispersed. For

8%/1% w/w (PAN/MWCNT), 0.40 g of PAN and 0.05 g of MWCNTs were dissolved in 4.55 g of DMF.

A custom-built electrospinning setup with a rotating drum collector was used to produce the nanofibers, shown in Figure 3.1. The solution was loaded into a 1 mL syringe equipped with a conductive, 21-gauge needle (Jensen Global, Catalog Number: JG21-1.0X). A high potential (+18 kV) was applied at the needle to the grounded collector with a fixed needle-to-collector distance of 15 cm using a commercially available high voltage source (Analog Technologies Inc, Catalog Number: AHVAC30KVR5MABT). A syringe pump (New Era, USA) was used to pump the solution (0.5 mL/hr) to maintain the steady Taylor cone. The collector rotation speed was set at 500 rpm to obtain randomly oriented fibers.

The nanofiber mats were mechanically compressed (Dayton's DC Speed Control Roller) five times and stabilized at 280 °C in air for 6 h. Following stabilization, the nanofiber mats were pyrolyzed in a tube furnace (Lindberg Blue M1100) with N_2 (9,000 SCCM) at 1000 °C (ramp rate of 2.5 °C/min) for 1 h and allowed to naturally cool to obtain the final carbon nanofiber material.

The resulting carbon nanofiber mats were cut (1 cm x 1 cm) and secured onto glass coverslips (12 mm) using PDMS. For electrically active scaffolds, a small amount of carbon paint was used to join a copper wire to the MSS. The junction was passivated with a sufficient amount of PDMS ensuring that the carbon paint and copper wire did not contribute to any obtained electrochemical signals.

3.2.2 Electrochemical Detection

Electrochemical tests were carried out using a Princeton Applied Research VersaSTAT 4 Potentiostat. To calibrate electrochemical measurements, the surface area of the electrode must

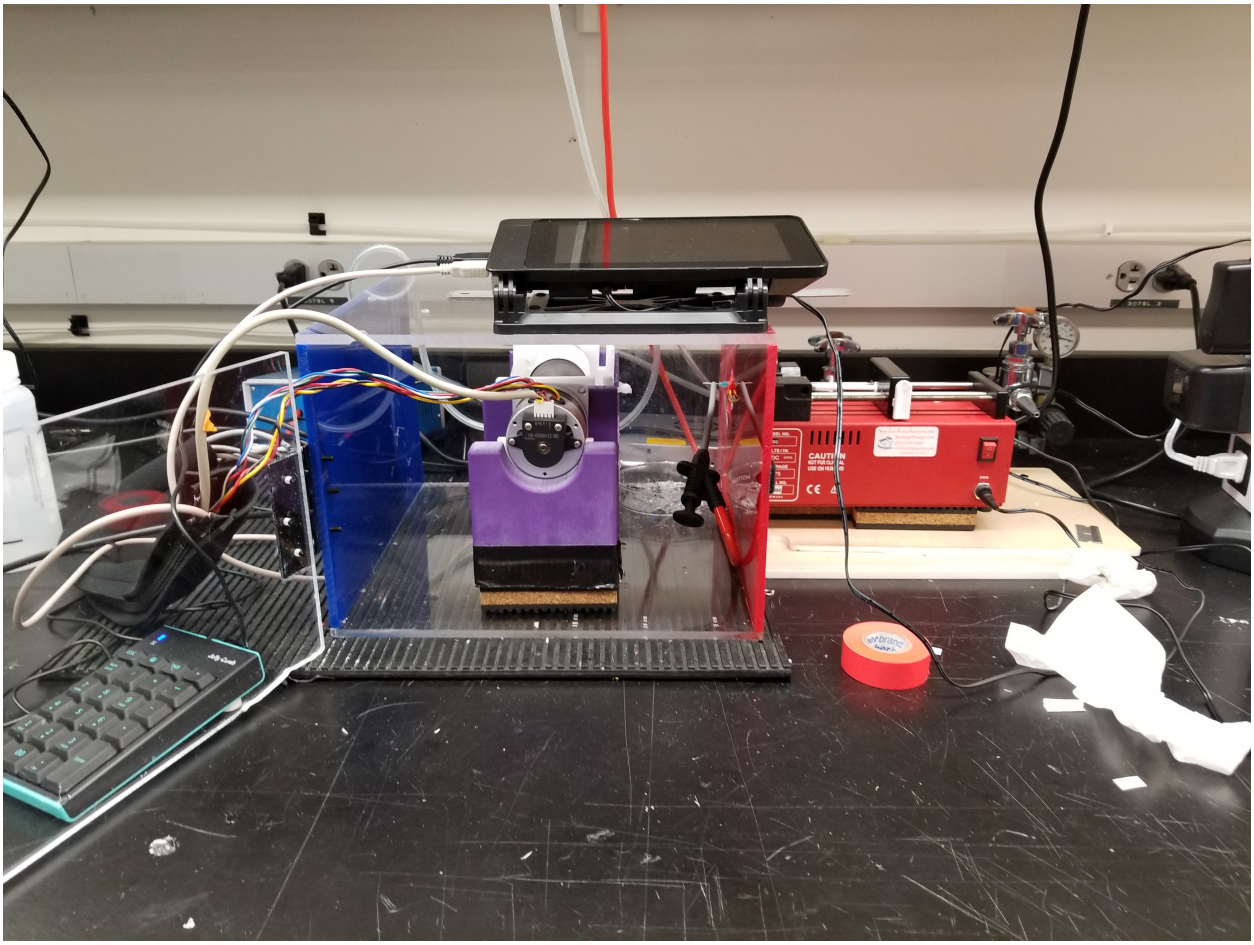

Figure 3.1: The custom made elecrtrospinning setup, showing the syringe setup and rotating drum.

be calculated. For simple, 2-dimensional electrodes, this is typically done using the Randles-Sevick equation (53). Since the electrospun carbon MSS was a complex, 3-dimensional material, electrochemical impedance spectroscopy (EIS) was used to find the double layer specific capacitance and calculate the electroactive surface area of each electrode using the following Equation 1:

$$S_{active} = \frac{I_c}{C_{dl} \cdot v} \tag{3.1}$$

where C_{dl} is the double layer capacitance, I_C is the capacitive current, and v is the scan rate. EIS was performed (10,000 Hz–0.1 Hz) in a blank electrolyte solution (PBS 0.1 M). The EIS Nyquist plot was fit with an equivalent electrical circuit and the resulting capacitance was normalized with the geometric surface area of the electrode. I_C and v were found using cyclic voltammetry.

ΔE_p was obtained by measuring the potential separation between the oxidation and reduction peaks at a scan rate of 50 mV/s. After verifying the linearity between the peak current and square root of the scan rate, k_0 was calculated according to the Nicholson method (53),(56),(57). The sensitivity of each electrode was calculated by taking the slope of the DPV calibration plot and the limit of detection was calculated using Equation 2:

$$LOD = \frac{3\sigma}{S} \tag{3.2}$$

where σ is the standard deviation of the background current signal in PBS (0.1 M) and S is the sensitivity of the electrode.

3.2.3 Material Characterization

Raman spectroscopy was performed using a Renishaw InVia Raman Microscope. Raman spectra was obtained using a 532-nm excitation laser and fit to Lorentzian peaks for analysis. The ID/IG ratio was calculated from the absolute peak intensities of the ID and IG Raman bands. SEM analysis was performed using an FEI Magellan 400 SEM.

3.3 Results and Discussion

3.3.1 Materials Characterization

Unlike other highly sensitive, electrochemical biosensors which require expensive and laborious fabrication techniques, we fabricate our carbon nanofiber mat by simply electrospinning an inexpensive polymer precursor solution consisting of polyacrylonitrile (PAN) and multi-walled carbon nanotubes (MWCNTs). The resulting polymer nanofibers are then pyrolyzed into carbon. While carbon electrodes have a wide electrochemical stability window, their sensitivity and electrochemical performance are highly dependent on their nanostructure. For example, while highly oriented pyrolytic graphitic (HOPG) carbon performs more similar to platinum, glassy carbon obtained from the pyrolysis of polymer precursors (like PAN), generally functions as a poor electrocatalytic, electrochemical sensor (50; 58). Several key steps in the fabrication process of the carbon electrode contribute to its improved electrochemical sensitivity for DA detection. The addition of MWCNTs to PAN templates and uncoils the PAN polymer chains, leading to a more conductive and fragmented graphitic nanostructure (27; 28). Stirring the PAN-MWCNT solution further enhances this process by generating microscopic drag forces between the surface-attracted polymer chains and the bulk polymer solution (29; 51). During the subsequent electrospinning process, shear forces

between the MWCNTs and polymer chains, traveling at different velocities within the fiber jet, continue to unwind the polymer. Compression of the material, followed by stabilization at the glass transition temperature (300 °C), preserves the templated PAN molecules in their uncoiled state (27).

Finally, pyrolysis of PAN in an inert environment, at relatively low temperatures (1000 °C), retains native nitrogen within the carbon nanofiber matrix, creating additional electrocatalytic sites for DA-enhanced adsorption and electrochemical activity (59). The fabrication process permanently embeds the favorable electroactive sites into the carbon nanostructure, an advantage over the typical carbon electrochemical sensor, which requires tedious surface functionalization or mechanical exfoliation to temporarily activate sites for detection. Since carbon MSS does not require any additional activation processes and exhibits an inherent electrochemical detectability, it is naturally advantageous for Dopamine detection in complex body fluids, where an electrode is required to retain active sites following several days or weeks in liquid culture.

To understand the effect of MWCNT loading on the material properties and electrochemical performance toward DA detection, we fabricated nanofiber carbon scaffolds with the following MWCNT loading amounts: (i) Pure PAN and (ii) 1% MWCNT/PAN. X-ray photoelectron spectroscopy (XPS) analysis was performed to verify that a high percentage of nitrogen groups were retained on the surface across both of the scaffolds (Figure 3.2a). Although nitrogen defects do not directly contribute to the redox activity towards DA, they promote adsorption of DA onto the electrode surface (59).

We used Raman spectroscopy to evaluate the composite carbon nanostructure by comparing the Raman intensity between the D and G band (I_D/I_G). The D band (1380 cm-1) in Raman spectra represents defects in sp^2 hybridized carbon, commonly found in amorphous carbon, while the G band (1580 cm-1) is associated with the ordered sp^2 C-C vibrational mode (60). As shown in Figure 3.2, an average I_D/I_G ratio of 1.115 +/- 0.077 found for pure

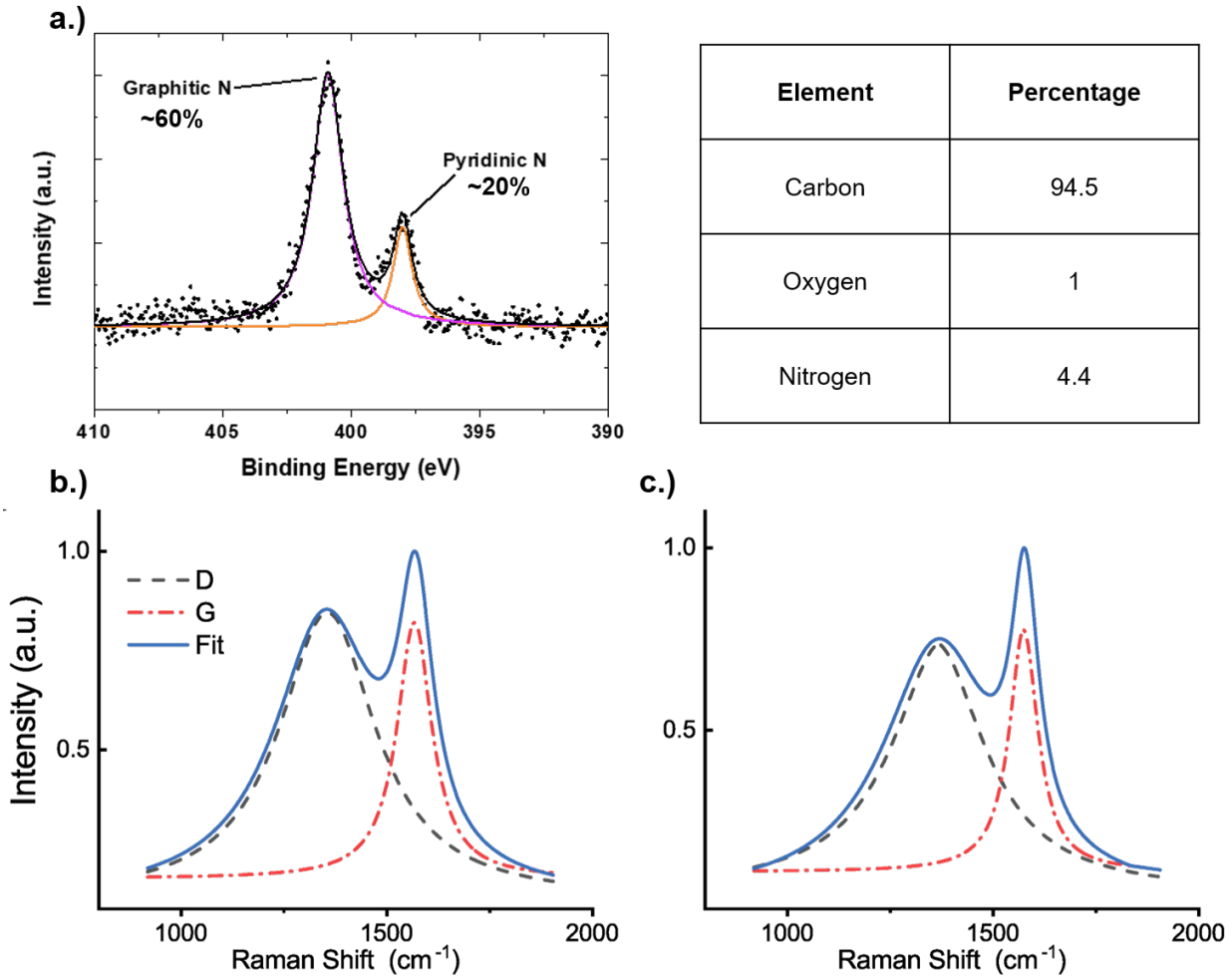

Element	Percentage
Carbon	94.5
Oxygen	1
Nitrogen	4.4

Figure 3.2: (a) Representative XPS distribution of the nitrogen groups found in the pyrolyzed carbon, with a table showing the approximate percentage of each element in the carbon. Average Raman spectra of the resulting carbon structures obtained after pyrolysis of (b) PAN and (c) 1% MWCNT/PAN.

PAN indicates an isotropically amorphous carbon (Figure 3.2b), while the addition of 1% MWCNT showed an average I_D/I_G ratio to 1.026 +/- 0.109, resulting in a less uniform carbon structure with regions of graphitic carbon embedded in bulk amorphous carbon (Figure 3.2c).

However, while the MWCNT does improve the degree of graphitization of the material, pure MWCNTs are generally not suited for electrochemical applications due to the predominance of inactive basal planes over the electrochemically more favorable edge planes (14; 12). To enhance electrochemical kinetics, one needs sufficient MWCNT loading to unwind PAN polymer chains and to feature enough graphitic edge planes while minimizing MWCNT agglomeration and basal planes. Therefore, we hypothesized that the inherently fragmented graphitic structure of our 1% MWCNT/PAN electrode would be create an ideal structure for the sensitive detection of DA and would be a better sensor than the pure PAN electrode, with little to no graphitic edge planes (27),(12).

3.3.2 Electrochemical Characterization

Cyclic Voltammetry

To determine the electrochemical performance of the pure PAN and 1% MWCNT/PAN carbon fiber nanostructures, we tested the electrode materials using chemically synthesized DA. Cyclic voltammetry allowed us to determine the reaction kinetics of each material and its response to DA (Figure 3.3 and Figure 3.4a). The separation between the reduction and oxidation peaks at different scan rates provides insight into the reversibility and kinetics of our system. In an ideal situation, the peak separation will remain constant regardless of the scan rate. The largest peak separation is observed for the pure PAN electrodes (265 mV separation) and the lowest is observed for the 1% MWCNT electrode (60 mV separation), indicating significantly more sluggish kinetics for the pure PAN materials over the 1% MWCNT electrode. To quantify the electrode kinetics, the heterogeneous electron

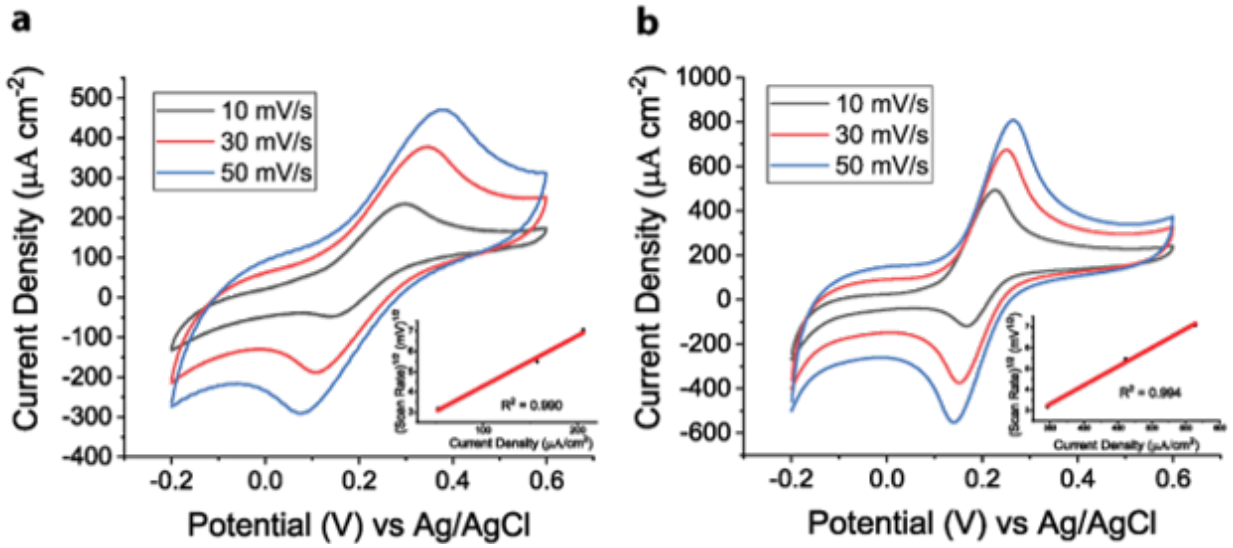

Figure 3.3: Cyclic voltammagrams of two different carbon nanofiber materials a) Pure PAN and b) 1% MWCNT/PAN at scan rates ranging from 0.01 V/s − 0.05 V/s. Inset graphs show the relationship between the peak current and the square root of the scan rate for all CV's. Linear fits for the calibration plots reveal linear response ($R^2 > 0.990$) for both electrode materials.

transfer rate, k^0, was estimated for each system using the procedure described by Nicholson (56; 12). As hypothesized, the k^0 for the 1% MWCNT/PAN electrode yielded the most favorable electrochemical kinetics, with k^0 values 4 times that of the pure PAN electrodes (0.0091 cm/s vs 0.00381 cm/s).

Differential Pulse Voltammetry

To quantitatively analyze the sensitivity and limit of detection of our chosen 1% MWCNT/PAN electrode material, we used differential pulse voltammetry (DPV), a highly sensitive voltammetric technique that can yield high signal-to-noise ratios at low concentrations of analyte by decoupling the capacitive, double-layer charging from the faradaic response. DPV was performed while gradually increasing the concentration of dopamine and measuring the resulting peak current (Figure 3.4a). The calibration plot (Figure 3.4b) shows a highly linear relationship between analyte concentration and the current peak height ($R^2 > 0.99$) allow-

	ΔE_p (mV)	k_0 (cm s^{-}1)	Sensitivity μA cm^{-}2	LOD (μM)
Pure PAN	301	0.00381	1.99	1.17
1% MWCNT/PAN	60	0.0091	5.57	0.393

Table 3.1: Comparison of electrochemical kinetics for the two different carbon nanofiber materials.

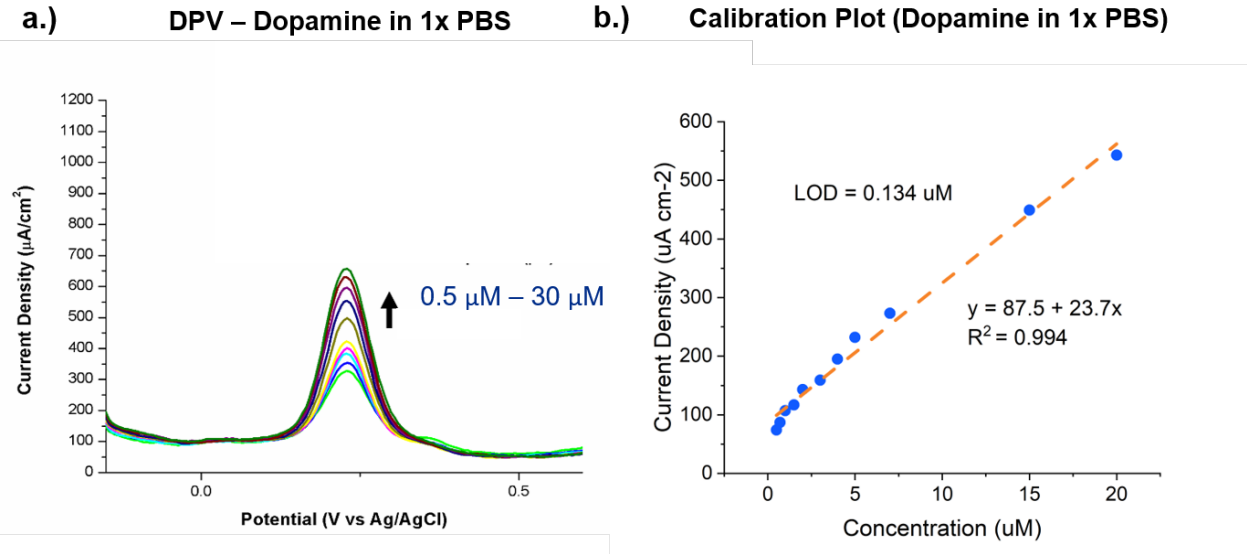

Figure 3.4: (a) DPV of the electrode material performance for the 1% MWCNT/PAN carbon nanofiber mat. (b) The linear correlation plot between concentration (x-axis, μM) and current density (y-axis, μA cm-2).

ing us to calculate the sensitivity and limit of detection of the electrode from the slope of the calibration plot and background standard deviation, Table 3.1. The 1% MWCNT/PAN electrode exhibited a limit-of-detection (LOD) of 0.134 μM (134 nM), comparable to the detection limits observed on noble metal-based electrodes and an order of magnitude lower than the LOD of pure PAN electrodes (1.17 μM). The excellent performance of the 1% MWCNT/PAN electrode suggests the 1% loading yields a high ratio of atomic edge planes over basal planes, creating a highly reactive and electrochemically favorable carbon surface.

3.3.3 Dopamine detection in the presence of interfering ions

Carbon electrodes traditionally have subpar performance for simultaneous detection of AA, UA, and DA because the electrochemical responses for these analytes generally overlaps. Typically, the degree of separation between the peak potentials of AA, UA, and DA directly correlates with the heterogenous electron rates (12). For carbons lacking an adequate quantity of strong adsorption sites (such as glassy carbon) the sluggish electron transfer kinetics results in a drastic positive shift in oxidation peak potential for all three species, causing their response to overlap and become indiscernible. As the surface of carbon is modified to enhance the adsorption and electron transfer kinetics of the three species, the individual oxidation peaks of each species undergo a negative potential shift, differentiating them from each other, as shown in Figure 3.5 (11), (42).

For the PAN-CNT carbon electrode, superior kinetics is evident from the appearance of the AA and DA peaks at much lower potentials than the UA peak, Figure 3.5c. This is absent in cyclic voltammograms for glassy carbon and pure PAN electrodes. In the glassy carbon electrode, the AA and DA peaks have shifted toward positive potentials due to slower kinetics of the electrode, creating a single discernible peak around 300 mV, see Figure 3.5a. For the pure PAN electrode, a clear peak is seen around 270 mV and a smaller, second peak is seen around 315 mV, shown in Figure 3.5b. The disappearance of the AA peak indicates the slower kinetics is forcing competition among the three electroactive species for electron transfer at the electrodes active sites. The improved kinetics in the PAN-CNT electrode results in an average peak separation difference of 195mV between the AA and DA peaks (ΔE_{UA-AA}), and 120mV between the DA and UA peaks (ΔE_{UA-AA}). Furthermore, these peak separations are comparable to those seen in prior studies on graphene-based electrodes (11), (42). The distinguishable electrochemical response and lack of interference between the electroactive species makes this material a superior platform for detection of DA in the presence of UA and AA.

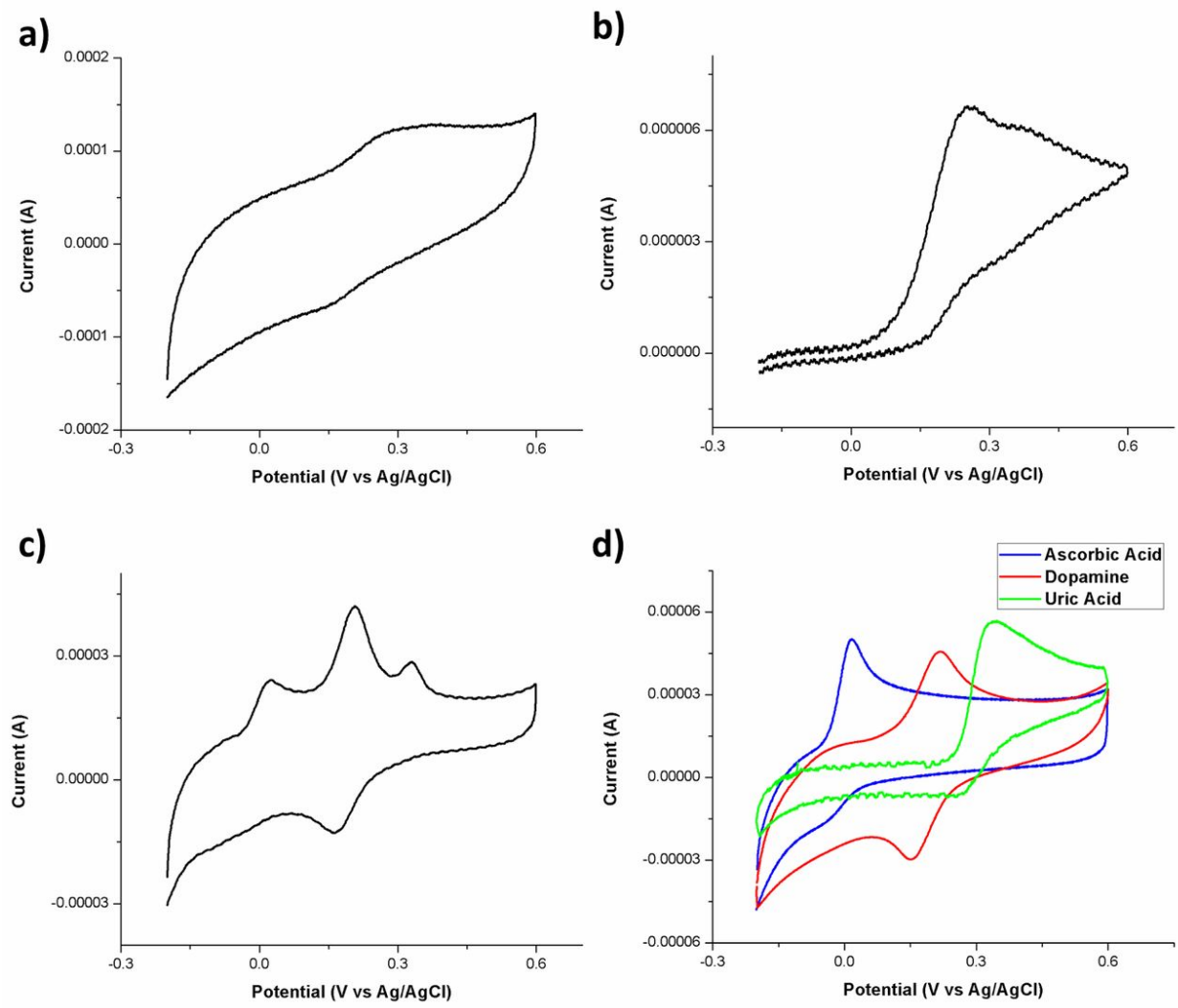

Figure 3.5: Cyclic voltammograms of a) glassy carbon, b) pure PAN electrode and c) treated CNT-PAN in 10 mM Ascorbic Acid, 1 mM Uric Acid and 1mM Dopamine in a pH 7.2 PBS buffer. d.) separate voltammograms were obtained of each electroactive species and the results were overlaid.

3.4 Conclusion

The development of novel electrochemical sensors that are able to detect Dopamine in low concentrations and in the presence of common interfering ions has long been a goal for many researchers. Dopamine detection is critical for the diagnosis of many neurological and metabolic disorders, including Parkinsons and Alzheimers. The challenge is to develop sensors with electrochemical kinetics fast enough to distinguish between the electrochemical responses of overlapping analytes commonly present in sample together, such as Dopamine, uric acid, and ascorbic acid. In this work, a porous carbon nanofiber material was developed with a microstructure that was abundant in electrochemically favorable graphitic edge planes and that was also rich in nitrogen heteroatoms. This structure was used to detect DA with limits of detection comparable to noble-metal based electrodes and successfully distinguished the electrochemical response from DA, UA, and AA.

Chapter 4

Conclusion

In carbon MEMS, a simple polymer precursor is turned into unique shapes and three dimensional structures using simple fabrication methods and converted into carbon via pyrolysis. Carbon MEMS provides powerful tools that allows for the development of structures and features at the limits of microfabrication and that incorporate many of the carbon allotropes available. This allows researchers to tune the material and geometric properties of the carbon MEMS device to suit all kinds of applications including batteries, electrochemical sensors, capacitors, scaffolds for tissue engineering, and molecular electronics.

In the work presented, we used several carbon MEMS fabrication processes to develop a highly fragmented, graphitic carbon nanofiber material ideal for electrochemical sensing of biomolecules such as iodide and dopamine and to be used as a three dimensional conductive scaffold that optimizes the growth and differentiation of neural stem cells. The material was successfully used to detect Iodide in urine in the presence of confounding molecules and was also successfully able to detect Dopamine at low concentrations and in the presence of ascorbic and uric acid.

Since carbon is also an excellent, biocompatible material, it has applications as a scaffold

for the growth of cells, especially stem cells that require unique materials and stimuli for directed growth. Future work will include the optimization of the material for the growth of stem cells and simultaneous electrochemical detection of their metabolites. A biocompatible carbon platform with a tunable macrostructural geometry for controlled stem cell growth and an ideal microstructure for electrochemical monitoring of those stem cells will provide a unique and robust tool for scientists and tissue engineers.

Bibliography

[1] M. Tilli, M. Paulasto-Krockel, T. Motooka, and V. Lindroos, *Handbook of Silicon Based MEMS Materials and Technologies*. William Andrew, Sept. 2015. Google-Books-ID: kMvcBAAAQBAJ.

[2] K. Petersen, "Silicon as a mechanical material," *Proceedings of the IEEE*, vol. 70, pp. 420–457, May 1982.

[3] C. Wang and M. Madou, "From MEMS to NEMS with carbon," *Biosensors & Bioelectronics*, vol. 20, pp. 2181–2187, Apr. 2005.

[4] S. Ranganathan, R. McCreery, S. M. Majji, and M. Madou, "Photoresist-Derived Carbon for Microelectromechanical Systems and Electrochemical Applications," *Journal of The Electrochemical Society*, vol. 147, pp. 277–282, Jan. 2000.

[5] C. Wang, L. Taherabadi, G. Jia, S. Kassegne, J. V. Zoval, and M. J. Madou, "Carbon-MEMS architectures for 3d microbatteries," in *MEMS, MOEMS, and Micromachining*, vol. 5455, pp. 295–302, International Society for Optics and Photonics, Aug. 2004.

[6] E. Fuhrer, A. Bäcker, S. Kraft, F. J. Gruhl, M. Kirsch, N. MacKinnon, J. G. Korvink, and S. Sharma, "3d Carbon Scaffolds for Neural Stem Cell Culture and Magnetic Resonance Imaging," *Advanced Healthcare Materials*, vol. 7, no. 4, p. 1700915, 2018.

[7] S. Shah, P. T. Yin, T. M. Uehara, S.-T. D. Chueng, L. Yang, and K.-B. Lee, "Guiding Stem Cell Differentiation into Oligodendrocytes Using Graphene-Nanofiber Hybrid Scaffolds," *Advanced Materials*, vol. 26, no. 22, pp. 3673–3680, 2014.

[8] A. Perebikovsky, A. Hwu, A. Yale, M. Ghazinejad, and M. J. Madou, "Nanofibrous Carbon Multi-functional Smart Scaffolds for Simultaneous Cell Differentiation and Dopamine Detection," *ACS Biomaterials Science & Engineering*, Dec. 2019.

[9] D.-S. Kim, E.-S. Kang, S. Baek, S.-S. Choo, Y.-H. Chung, D. Lee, J. Min, and T.-H. Kim, "Electrochemical detection of dopamine using periodic cylindrical gold nanoelectrode arrays," *Scientific Reports*, vol. 8, pp. 1–10, Sept. 2018.

[10] R. Martinez-Duarte, "SU-8 Photolithography as a Toolbox for Carbon MEMS," *Micromachines*, vol. 5, pp. 766–782, Sept. 2014.

[11] N. G. Shang, P. Papakonstantinou, M. McMullan, M. Chu, A. Stamboulis, A. Potenza, S. S. Dhesi, and H. Marchetto, "Catalyst-Free Efficient Growth, Orientation and Biosensing Properties of Multilayer Graphene Nanoflake Films with Sharp Edge Planes," *Advanced Functional Materials*, vol. 18, no. 21, pp. 3506–3514, 2008.

[12] S. Holmberg, M. Ghazinejad, E. Cho, D. George, B. Pollack, A. Perebikovsky, R. Ragan, and M. Madou, "Stress-activated pyrolytic carbon nanofibers for electrochemical platforms," *Electrochimica Acta*, vol. 290, pp. 639–648, Nov. 2018.

[13] M. J. Madou, V. H. Perez-Gonzalez, and B. Pramanick, *Carbon: The Next Silicon?: Book 1 - Fundamentals*. Momentum Press, Jan. 2016. Google-Books-ID: IPxdCwAAQBAJ.

[14] R. L. McCreery, "Advanced Carbon Electrode Materials for Molecular Electrochemistry," *Chemical Reviews*, vol. 108, pp. 2646–2687, July 2008.

[15] C. Wang, R. Zaouk, B. Y. Park, and M. J. Madou, "Carbon as a MEMS material: micro and nanofabrication of pyrolysed photoresist carbon," *International Journal of Manufacturing Technology and Management*, vol. 13, pp. 360–375, Jan. 2008.

[16] O. J. A. Schueller, S. T. Brittain, C. Marzolin, and G. M. Whitesides, "Fabrication and Characterization of Glassy Carbon MEMS," *Chemistry of Materials*, vol. 9, pp. 1399–1406, June 1997.

[17] P. J. F. Harris, "Fullerene-related structure of commercial glassy carbons," *Philosophical Magazine*, vol. 84, no. 29, pp. 3159–3167, 2004.

[18] C. Wang and M. Madou, "From MEMS to NEMS with carbon," *Biosensors and Bioelectronics*, vol. 20, pp. 2181–2187, Apr. 2005.

[19] L. Amato, A. Heiskanen, C. Caviglia, F. Shah, K. Zór, M. Skolimowski, M. Madou, L. Gammelgaard, R. Hansen, E. G. Seiz, M. Ramos, T. R. Moreno, A. Martínez-Serrano, S. S. Keller, and J. Emnéus, "Pyrolysed 3d-Carbon Scaffolds Induce Spontaneous Differentiation of Human Neural Stem Cells and Facilitate Real-Time Dopamine Detection," *Advanced Functional Materials*, vol. 24, no. 44, pp. 7042–7052, 2014.

[20] C. Wang, G. Jia, L. Taherabadi, and M. Madou, "A novel method for the fabrication of high-aspect ratio C-MEMS structures," *Journal of Microelectromechanical Systems*, vol. 14, pp. 348–358, Apr. 2005.

[21] B. Y. Park, R. Zaouk, C. Wang, and M. J. Madou, "A Case for Fractal Electrodes in Electrochemical Applications," *Journal of The Electrochemical Society*, vol. 154, pp. P1–P5, Feb. 2007.

[22] S. Jin, H. Deng, D. Long, X. Liu, L. Zhan, X. Liang, W. Qiao, and L. Ling, "Facile synthesis of hierarchically structured Fe3o4/carbon micro-flowers and their application to lithium-ion battery anodes," *Journal of Power Sources*, vol. 196, pp. 3887–3893, Apr. 2011.

[23] R. R. Kamath and M. J. Madou, "Three-Dimensional Carbon Interdigitated Electrode Arrays for Redox-Amplification," *Analytical Chemistry*, vol. 86, pp. 2963–2971, Mar. 2014.

[24] A. L. Yarin, S. Koombhongse, and D. H. Reneker, "Taylor cone and jetting from liquid droplets in electrospinning of nanofibers," *Journal of applied physics*, vol. 90, no. 9, pp. 4836–4846, 2001.

[25] M. J. Madou, *Fundamentals of microfabrication: the science of miniaturization*. CRC press, 2002.

[26] S. Sharma, A. Sharma, Y.-K. Cho, and M. Madou, "Increased graphitization in electrospun single suspended carbon nanowires integrated with carbon-MEMS and carbon-NEMS platforms," *ACS applied materials & interfaces*, vol. 4, no. 1, pp. 34–39, 2012.

[27] M. Ghazinejad, S. Holmberg, O. Pilloni, L. Oropeza-Ramos, and M. Madou, "Graphitizing Non-graphitizable Carbons by Stress-induced Routes," *Scientific Reports*, vol. 7, p. 16551, Nov. 2017.

[28] T. Maitra, S. Sharma, A. Srivastava, Y.-K. Cho, M. Madou, and A. Sharma, "Improved graphitization and electrical conductivity of suspended carbon nanofibers derived from carbon nanotube/polyacrylonitrile composites by directed electrospinning," *Carbon*, vol. 50, pp. 1753–1761, Apr. 2012.

[29] N. Tajaddod, H. Li, and M. L. Minus, "Low-temperature graphitic formation promoted by confined interphase structures in polyacrylonitrile/carbon nanotube materials," *Polymer*, vol. 137, pp. 346–357, Feb. 2018.

[30] F. Delange, "The disorders induced by iodine deficiency," *Thyroid: Official Journal of the American Thyroid Association*, vol. 4, no. 1, pp. 107–128, 1994.

[31] B. de Benoist, E. McLean, M. Andersson, and L. Rogers, "Iodine deficiency in 2007: global progress since 2003," *Food and Nutrition Bulletin*, vol. 29, pp. 195–202, Sept. 2008.

[32] W. H. Organization, "Urinary iodine concentrations for determining iodine status in populations," 2013.

[33] C. P. Shelor and P. K. Dasgupta, "Review of analytical methods for the quantification of iodine in complex matrices," *Analytica Chimica Acta*, vol. 702, pp. 16–36, Sept. 2011.

[34] M. Haap, H. J. Roth, T. Huber, H. Dittmann, and R. Wahl, "Urinary iodine: comparison of a simple method for its determination in microplates with measurement by inductively-coupled plasma mass spectrometry," *Scientific Reports*, vol. 7, p. 39835, Jan. 2017.

[35] Z. H. Ibupoto, K. Khun, and M. Willander, "A Selective Iodide Ion Sensor Electrode Based on Functionalized ZnO Nanotubes," *Sensors*, vol. 13, pp. 1984–1997, Feb. 2013.

[36] X. Xu and Y. Wang, "A Novel Sensor for Sensitive and Selective Detection of Iodide Using Turn-on Fluorescence Graphene Quantum Dots/Ag Nanocomposite," *Analytical Sciences: The International Journal of the Japan Society for Analytical Chemistry*, vol. 31, no. 8, pp. 787–791, 2015.

[37] R.-H. Yang, K.-M. Wang, D. Xiao, and X.-H. Yang, "Development of an iodine sensor based on fluorescence energy transfer," *Analyst*, vol. 125, pp. 1441–1445, Jan. 2000.

[38] T. R. I. Cataldi, A. Rubino, M. C. Laviola, and R. Ciriello, "Comparison of silver, gold and modified platinum electrodes for the electrochemical detection of iodide in urine samples following ion chromatography," *Journal of Chromatography B*, vol. 827, pp. 224–231, Dec. 2005.

[39] B. Dielacher, R. F. Tiefenauer, J. Junesch, and J. Vörös, "Iodide sensing via electrochemical etching of ultrathin gold films," *Nanotechnology*, vol. 26, no. 2, p. 025202, 2015.

[40] E. R. Lowe, C. E. Banks, and R. G. Compton, "Edge Plane Pyrolytic Graphite Electrodes for Halide Detection in Aqueous Solutions," *Electroanalysis*, vol. 17, pp. 1627–1634, Sept. 2005.

[41] B. Pollack, S. Holmberg, D. George, I. Tran, M. Madou, and M. Ghazinejad, "Nitrogen-Rich Polyacrylonitrile-Based Graphitic Carbons for Hydrogen Peroxide Sensing," *Sensors*, vol. 17, p. 2407, Oct. 2017.

[42] S.-M. Li, S.-Y. Yang, Y.-S. Wang, C.-H. Lien, H.-W. Tien, S.-T. Hsiao, W.-H. Liao, H.-P. Tsai, C.-L. Chang, C.-C. M. Ma, and C.-C. Hu, "Controllable synthesis of nitrogen-doped graphene and its effect on the simultaneous electrochemical determination of ascorbic acid, dopamine, and uric acid," *Carbon*, vol. 59, pp. 418–429, Aug. 2013.

[43] S. Kundu, T. C. Nagaiah, W. Xia, Y. Wang, S. V. Dommele, J. H. Bitter, M. Santa, G. Grundmeier, M. Bron, and W. Schuhmann, "Electrocatalytic activity and stability of nitrogen-containing carbon nanotubes in the oxygen reduction reaction," *The Journal of Physical Chemistry C*, vol. 113, no. 32, pp. 14302–14310, 2009.

[44] S. Lopez-Giacoman and M. Madero, "Biomarkers in chronic kidney disease, from kidney function to kidney damage," *World Journal of Nephrology*, vol. 4, pp. 57–73, Feb. 2015.

[45] A. Shrivastava and V. B. Gupta, "Methods for the determination of limit of detection and limit of quantitation of the analytical methods," *Chronicles of Young Scientists*, vol. 2, p. 21, Jan. 2011.

[46] L. Liu, H. Mo, S. Wei, and D. Raftery, "Quantitative analysis of urea in human urine and serum by 1h nuclear magnetic resonance," *The Analyst*, vol. 137, pp. 595–600, Feb. 2012.

[47] D. B. Barr, L. C. Wilder, S. P. Caudill, A. J. Gonzalez, L. L. Needham, and J. L. Pirkle, "Urinary Creatinine Concentrations in the U.S. Population: Implications for Urinary Biologic Monitoring Measurements," *Environmental Health Perspectives*, vol. 113, pp. 192–200, Feb. 2005.

[48] "WHO | Iodine status worldwide."

[49] H. Bernheimer, W. Birkmayer, O. Hornykiewicz, K. Jellinger, and F. Seitelberger, "Brain dopamine and the syndromes of Parkinson and Huntington Clinical, morphological and neurochemical correlations," *Journal of the Neurological Sciences*, vol. 20, pp. 415–455, Dec. 1973.

[50] A. N. Patel, S.-y. Tan, T. S. Miller, J. V. Macpherson, and P. R. Unwin, "Comparison and Reappraisal of Carbon Electrodes for the Voltammetric Detection of Dopamine," *Analytical Chemistry*, vol. 85, pp. 11755–11764, Dec. 2013.

[51] J.-H. Lee, H. K. Choi, L. Yang, S.-T. D. Chueng, J.-W. Choi, and K.-B. Lee, "Nondestructive Real-Time Monitoring of Enhanced Stem Cell Differentiation Using a Graphene-Au Hybrid Nanoelectrode Array," *Advanced Materials*, vol. 30, no. 39, p. 1802762, 2018.

[52] S. E. Marsh and M. Blurton-Jones, "Neural stem cell therapy for neurodegenerative disorders: The role of neurotrophic support," *Neurochemistry International*, vol. 106, pp. 94–100, June 2017.

[53] D. A. C. Brownson and C. E. Banks, *The Handbook of Graphene Electrochemistry*. London: Springer-Verlag, 2014.

[54] H. Wang, T. Maiyalagan, and X. Wang, "Review on Recent Progress in Nitrogen-Doped Graphene: Synthesis, Characterization, and Its Potential Applications," *ACS Catalysis*, vol. 2, pp. 781–794, May 2012.

[55] R. J. Rice, N. M. Pontikos, and R. L. McCreery, "Quantitative correlations of heterogeneous electron-transfer kinetics with surface properties of glassy carbon electrodes," *Journal of the American Chemical Society*, vol. 112, pp. 4617–4622, June 1990.

[56] R. S. Nicholson, "Theory and Application of Cyclic Voltammetry for Measurement of Electrode Reaction Kinetics.," *Analytical Chemistry*, vol. 37, pp. 1351–1355, Oct. 1965.

[57] I. Lavagnini, R. Antiochia, and F. Magno, "An Extended Method for the Practical Evaluation of the Standard Rate Constant from Cyclic Voltammetric Data," *Electroanalysis*, vol. 16, pp. 505–506, Apr. 2004.

[58] D. A. C. Brownson, D. K. Kampouris, and C. E. Banks, "Graphene electrochemistry: fundamental concepts through to prominent applications," *Chemical Society Reviews*, vol. 41, no. 21, pp. 6944–6976, 2012.

[59] J. A. Behan, M. K. Hoque, S. N. Stamatin, T. S. Perova, L. Vilella-Arribas, M. García-Melchor, and P. E. Colavita, "Experimental and Computational Study of Dopamine as an Electrochemical Probe of the Surface Nanostructure of Graphitized N-Doped Carbon," *The Journal of Physical Chemistry C*, vol. 122, pp. 20763–20773, Sept. 2018.

[60] A. C. Ferrari and J. Robertson, "Interpretation of Raman spectra of disordered and amorphous carbon," *Physical Review B*, vol. 61, pp. 14095–14107, May 2000.